Open access • Journal Article • DOI:10.1109/78.960415

Biorthogonal Butterworth wavelets derived from discrete interpolatory splines

Amir Averbuch, Alexander B. Pevnyi, Valery A. Zheludev

Institutions: Tel Aviv University

Published on: 01 Nov 2001 - IEEE Transactions on Signal Processing (IEEE)

Topics: Biorthogonal wavelet, Biorthogonal system, Lifting scheme, Wavelet and Fast Fourier transform

Biorthogonal Butterworth Wavelets Derived from Discrete Interpolatory Splines

Amir Z. Averbuch, Alexander B. Pevnyi, and Valery A. Zheludev

***Abstract*—In the paper, we present a new family of biorthogonal wavelet transforms and a related library of biorthogonal periodic symmetric waveforms. For the construction, we used the interpolatory discrete splines, which enabled us to design a library of perfect reconstruction filterbanks. These filterbanks are related to Butterworth filters. The construction is performed in a "lifting" manner. The difference from the conventional lifting scheme is that all the transforms are implemented in the frequency domain with the use of the fast Fourier transform (FFT). Two ways to choose the control filters are suggested. The proposed scheme is based on interpolation, and as such, it involves only samples of signals, and it does not require any use of quadrature formulas. These filters have linear-phase property, and the basic waveforms are symmetric. In addition, these filters yield refined frequency resolution.**

***Index Terms*—Biorthogonal wavelets, Butterworth filters, discrete splines, lifting scheme.**

I. Introduction

THE CONTINUOUS polynomial splines have a rich history as a source for wavelet constructions [3], [4], [6], [9], [18], [19], but only a few authors [10], [13] use the discrete splines for this purpose. However, discrete splines are a natural tool for processing of discrete time signals. An intermediate approach can be found in [2], where the authors used the filters that originated from the sampled B-splines for the construction of the multiresolution analysis in l_2.

In this work, we employed the interpolatory periodic discrete splines [11] as a tool for devising a discrete biorthogonal wavelet scheme. The proposed construction is somewhat related to Donoho's interpolating wavelet construction [7] as it was modified later by Sweldens [16] into what is called the "lifting scheme." The lifting scheme allows custom design and fast implementation of the transforms. Briefly, the idea of the computation is that values of the signal located at odd positions are predicted by values in the midpoints of the spline that interpolates even values of the signal. Then, the odd subarray is replaced by the difference between the current and the predicted subarrays. On smooth well-correlated fragments of the signal, these differences will be near zero, whereas irregular fragments will produce significant differences. This result resembles the operation of the wavelet transform. To further extend this resemblance, we should employ the new odd subarray for updating the existing even subarray. The goal of this update is to smooth the even subarray and thus reduce the aliasing, which is a consequence of the decimation. Based on the above strategy, we constructed a new family of biorthogonal wavelet and wavelet packet transforms and a related library of biorthogonal symmetric waveforms. In [19], a similar approach was developed through the use of polynomial interpolatory splines as the predicting aggregate. In that paper as well as in the present one, all the computations are conducted in the frequency domain using FFT.

Our construction results in a perfect reconstruction filterbank that is linear phase. The corresponding wavelets are symmetric. Our investigation revealed an interesting relation between the decomposition splines and the Butterworth filters [12] commonly used in signal processing. The filterbanks constructed in the paper comprise filters that act as bidirectional (forward and backward) halfband Butterworth filters. The frequency response of Butterworth filters are maximally flat, and we succeeded in construction of the dual filters with similar property. A few schemes were reported in the literature where the one-pass Butterworth filters were used for devising an orthogonal nonsymmetric wavelets [1], [8], [15], [17]. Corresponding wavelets were called the biorthogonal Butterworth wavelets. To distinguish the wavelets constructed in our scheme from the former ones, we name our wavelets the *biorthogonal Butterworth wavelets*.

The paper is organized as follows. In Section II, we outline some facts about the discrete splines and the periodic Butterworth filters. In Section III, we devise a family of biorthogonal wavelet-type transforms of signals using lifting steps. The lifting scheme that we propose operates in the frequency domain, contrary to the conventional lifting scheme. Both the primal and dual schemes for construction are considered. We emphasize the fact that the lifting scheme together with the proposed construction yields an efficient computational algorithm. Section IV is devoted to the description of the properties of the constructed filterbanks and basic elements of the transforms. The filterbanks contain some control tools that allow custom design of the wavelets. In the end of the section, we show how to use these control tools. The transforms that were presented in Section III are one-level (scale) wavelet-type transforms. They can be extended into coarser scales in two ways. One way is to use the multiscale wavelet transform when the frequency domain is split in logarithmic fashion. Another way is to use the wavelet packet transform when the partition of the frequency domain is near uniform and it is being refined in each subsequent scale of the transform. We describe in Section V the wavelet-type

Manuscript received August 18, 2000; revised August 1, 2001. This work was supported in part by the Israel Science Foundation, 1999–2003, under Grant 258/99-1, "Application of the Wavelet Transform to 3D Seismic Imaging." The associate editor coordinating the review of this paper and approving it for publication was Prof. Paulo S. R. Diniz.

A. Z. Averbuch and V. A. Zheludev are with the School of Computer Sciences, Tel-Aviv University, Tel-Aviv, Israel (e-mail: amir@math.tau.ac.il; zhel@math.tau.ac.il).

A. B. Pevnyi is with the Department of Mathematics, Syktyvkar University, Syktyvkar, Russia (e-mail: pevnyi@ssu.edu.komi.ru).

Publisher Item Identifier S 1053-587X(01)09243-1.

transform. Throughout the paper, we present a wide collection of filterbanks, wavelets, and their spectra.

II. Preliminaries

A. Discrete Periodic Splines

In this section, we outline briefly the properties of discrete periodic splines that are needed for further constructions. For detailed description of the subject, see [11].

Throughout the paper, we assume that m, n, and t are natural numbers and that $mn = N = 2^t$. Denote $\omega_N = e^{2\pi j/N}$. The discrete Fourier transform (DFT) of an array $\{a(k)\}_{k=0}^{N-1}$, which we denote $\{\hat{a}^N(\nu)\}_{\nu=0}^{N-1}$, and its inverse (IDFT) are

$$\hat{a}^N(\nu) = \sum_{k=0}^{N-1} \omega_N^{-\nu k} a(k)$$

$$a(k) = \frac{1}{N} \sum_{\nu=0}^{N-1} \omega_N^{\nu k} \hat{a}^N(\nu), \qquad \nu,\, k = 0, \ldots, N-1.$$

We recall the following properties of DFT:

$$\text{If } a(k) = \sum_{l=0}^{N-1} b(k-l)c(l) \text{ then } \hat{a}^N(\nu) = \hat{b}^N(\nu)\hat{c}^N(\nu) \tag{2.1}$$

$$\sum_{k=0}^{N/2-1} \omega_{N/2}^{-\nu k} a(2k) = \tfrac{1}{2}\left(\hat{a}^N(\nu) + \hat{a}^N(\nu + N/2)\right) \tag{2.2}$$

$$\sum_{k=0}^{N/2-1} \omega_{N/2}^{-\nu k} a(2k+1) = \frac{\omega_N^{\nu}}{2}\left(\hat{a}^N(\nu) - \hat{a}^N(\nu + N/2)\right). \tag{2.3}$$

Definition 2.1: The IDFT of the sequence

$$q_{r,m,n}(\nu) = \begin{cases} n^{2r} & \text{if } \nu = 0 \\ \left(\dfrac{\sin \pi\nu/m}{\sin \pi\nu/N}\right)^{2r} & \text{if } \nu = 1, \ldots N-1: \end{cases}$$

$$Q_{r,m,n}(k) = \frac{1}{N} \sum_{\nu=0}^{N-1} \omega_N^{\nu k} q_{r,m,n}(\nu)$$

is called the (m, n) discrete periodic B-spline of order $2r$.

The (m, n) discrete periodic spline of order $2r$ is defined as a linear combination, with real-valued coefficients, of shifts of the (m, n) B-spline of order $2r$:

$$S_{r,m,n}(k) = \sum_{l=0}^{m-1} c(l) Q_{r,m,n}(k - nl).$$

In the paper, we are interested only in the case when $m = N/2$ and $n = 2$. The corresponding splines are denoted as $Q_r = Q_{r,N/2,2}$ and $S_r = S_{r,N/2,2}$. In this case, we have

$$Q_r(k) = \frac{1}{N} \sum_{\nu=0}^{N-1} \omega_N^{\nu k} \left(2\cos\frac{\nu\pi}{N}\right)^{2r}$$

$$S_r(k) = \sum_{l=0}^{m-1} c(l) Q_r(k - 2l). \tag{2.4}$$

Definition 2.2: Let $\{e(k)\}$, $k \in 0, \ldots, m-1$ be a given sequence. The discrete periodic spline S_r is called the interpolatory spline if the following relations hold:

$$S_r(2k) = e(k), \qquad k \in 0, \ldots, m-1. \tag{2.5}$$

The points $\{2k\}$ are called the nodes of the spline.

The interpolatory splines of any order can be explicitly constructed.

Proposition 2.1: The interpolatory spline that satisfies (2.5) is represented as follows:

$$S_r(k) = \sum_{l=0}^{m-1} c(l) Q_r(k - 2l),$$

$$c(l) = \sum_{\nu=0}^{m-1} \frac{2\omega_{N/2}^{\nu k} \hat{e}^m(\nu)}{\left(2\cos\dfrac{\nu\pi}{N}\right)^{2r} + \left(2\sin\dfrac{\nu\pi}{N}\right)^{2r}}, \quad m = N/2. \tag{2.6}$$

Proof: Let us rewrite (2.5) using (2.4)

$$\sum_{l=0}^{m-1} c(l) Q_r(2(k-l)) = e(k)$$

and apply the m-point DFT on both sides of this equation. From (2.2), it follows that the m-point DFT of the decimated B-spline is

$$\begin{aligned} \hat{Q}_r^m(\nu) &= \sum_{k=0}^{m-1} \omega_{N/2}^{-\nu k} Q_r(2k) \\ &= \tfrac{1}{2}\left(\hat{Q}_r^N(\nu) + \hat{Q}_r^N(\nu + m)\right) \\ &= \frac{1}{2}\left(\left(2\cos\frac{\nu\pi}{N}\right)^{2r} + \left(2\sin\frac{\nu\pi}{N}\right)^{2r}\right). \end{aligned}$$

Hence, we have, using (2.1)

$$\frac{1}{2}\left(\left(2\cos\frac{\nu\pi}{N}\right)^{2r} + \left(2\sin\frac{\nu\pi}{N}\right)^{2r}\right)\hat{c}^m(\nu) = \hat{e}^m(\nu).$$

■

For further development, we need to know the values of the splines in the midpoints between the nodes, which we denote as $\sigma(k) = S_r(2k+1)$, $k \in 0, \ldots, m-1$.

Proposition 2.2: The values of the interpolatory spline in the midpoints are

$$\sigma(k) = \frac{1}{m} \sum_{\nu=0}^{m-1} \omega_m^{\nu k} \hat{\sigma}^m(\nu)$$

$$\hat{\sigma}^m(\nu) = \hat{e}^m(\nu)\omega_N^{\nu} U_1(\nu) \tag{2.7}$$

$$U_1(\nu) = \frac{\left(\cos\dfrac{\nu\pi}{N}\right)^{2r} - \left(\sin\dfrac{\nu\pi}{N}\right)^{2r}}{\left(\cos\dfrac{\nu\pi}{N}\right)^{2r} + \left(\sin\dfrac{\nu\pi}{N}\right)^{2r}}$$

$$\nu,\, k = 0, \ldots, m-1. \tag{2.8}$$

The function U_1 is N-periodic and $U_1(\nu + m) = -U_1(\nu)$.

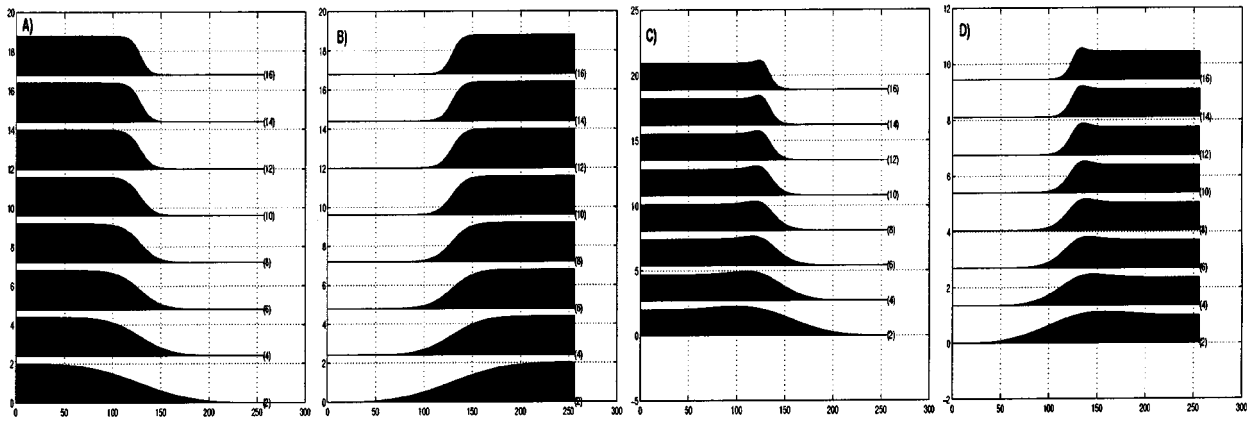

Fig. 1. (a) Lowpass filter functions h^1, which is the magnitude squared frequency-response functions of the lowpass halfband Butterworth filters of order $r = 1$ at the bottom to order $r = 8$ at the top. (b) Highpass filter functions $\bar{g}^1$, which is the magnitude squared frequency-response functions of the highpass halfband Butterworth filters. (c) Lowpass filter functions $h^1_{\tilde{\beta}}$ of order $r = 1$ at the bottom to order $r = 8$ at the top. (d) Highpass filter functions $g^1_{\tilde{\beta}}$.

Proof: Similarly to previous considerations, we apply the m-point DFT on both sides of the following equation:

$$\sigma(k) = \sum_{l=0}^{m-1} c(l) Q_r(2k+1-l).$$

From (2.3), we derive

$$\begin{aligned}\sum_{k=0}^{m-1} &\omega_{N/2}^{-\nu k} Q_r(2k+1) \\ &= \frac{\omega_N^{\nu}}{2}\left(\hat{Q}_r^N(\nu) - \hat{Q}_r^N(\nu+m)\right) \\ &= \frac{\omega_N^{\nu k}}{2}\left(\left(2\cos\frac{\nu\pi}{N}\right)^{2r} - \left(2\sin\frac{\nu\pi}{N}\right)^{2r}\right).\end{aligned}$$

Hence, using (2.6), we get

$$\begin{aligned}\hat{\sigma}^m(\nu) &= \frac{\omega_N^{\nu}}{2}\left(\left(2\cos\frac{\nu\pi}{N}\right)^{2r} - \left(2\sin\frac{\nu\pi}{N}\right)^{2r}\right)\hat{e}(\nu)^m\hat{c}(\nu)^m \\ &= \hat{e}^m(\nu)\omega_N^{\nu}U_1(\nu).\end{aligned}$$

■

B. Discrete Periodic Butterworth Filters

We recall briefly the notion of Butterworth filter. For details, see [12]. The input $x(n)$ and output $y(n)$ of a linear discrete time shift-invariant system are linked as follows:

$$y(n) = \sum_{k=-\infty}^{\infty} f(k)x(n-k). \tag{2.9}$$

Such a processing of the signal $x(n)$ is called digital filtering, and the sequence $f(n)$ is called the impulse response of the filter. Denote by $X(\omega) = \sum_{n=-\infty}^{\infty} e^{-i\omega n}x(n)$, $Y(\omega) = \sum_{n=-\infty}^{\infty} e^{-i\omega n}y(n)$, $F(\omega) = \sum_{n=-\infty}^{\infty} e^{-i\omega n}f(n)$ the Fourier transforms of the sequences. Then, we have from (2.9) $Y(\omega) = F(\omega)X(\omega)$. The function $F(\omega)$ is called the frequency response of the digital filter. The digital Butterworth filter is the filter with the maximally flat frequency response. The magnitude squared frequency responses $F_l(\omega)$ and $F_h(\omega)$ of the digital lowpass and highpass Butterworth filters of order r, respectively, are given by

$$|F_l(\omega)|^2 = \frac{1}{1+\left(\tan\frac{\omega}{2}\Big/\tan\frac{\omega_c}{2}\right)^{2r}}$$

$$|F_h(\omega)|^2 = 1 - |F_l(\omega)|^2 = \frac{1}{1+\left(\tan\frac{\omega_c}{2}\Big/\tan\frac{\omega}{2}\right)^{2r}}$$

where ω_c is the so-called cutoff frequency.

We are interested in the halfband Butterworth filters that is $\omega_c = \pi/2$. In this case

$$|F_l(\omega)|^2 = \frac{1}{1+\left(\tan\frac{\omega}{2}\right)^{2r}}$$

$$|F_h(\omega)|^2 = 1 - |F_l(\omega)|^2 = \frac{1}{1+\left(\cot\frac{\omega}{2}\right)^{2r}}.$$

When the signals x and y and the impulse response f are N-periodic, the linear convolution in (2.9) becomes circular, and in subsequent formulas, ω is replaced by $2\nu\pi/N$. In particular, the magnitude squared frequency responses of the digital periodic lowpass and highpass Butterworth filters of order r are given by the formulas

$$|F_l(\nu)|^2 = \frac{1}{1+\left(\tan\frac{\nu\pi}{N}\right)^{2r}}$$

$$|F_h(\omega)|^2 = 1 - |F_l(\omega)|^2 = \frac{1}{1+\left(\cot\frac{\nu\pi}{N}\right)^{2r}}. \tag{2.10}$$

These functions for various r are displayed in Fig. 1.

III. Biorthogonal Transforms

We introduce a family of biorthogonal wavelet-type transforms that operate on the signal $\mathbf{x} = \{x(k)\}$, $k = 0, \ldots N-1$, which we construct through lifting steps. The significant difference with the conventional lifting scheme [16] lies in the fact that here, we operate in the frequency domain.

The lifting scheme can be implemented in a primal or dual modes. We consider both.

A. Primal Scheme

1) Decomposition: Generally, the lifting scheme for decomposition of signals consists of three steps:

1) split;
2) predict;
3) update or lifting.

Let us construct and implement our proposed schemes in terms of these steps.

Split: We simply split the array $\mathbf{x}$ into an even and odd subarrays

$$\mathbf{e_1} = \{e_1(k) = x(2k)\},$$
$$\mathbf{d_1} = \{d_1(k) = x(2k+1)\}, \quad k \in 0, \ldots, m-1;\ m = N/2.$$

Predict: We use the even array $\mathbf{e_1}$ to predict the odd array $\mathbf{d_1}$ and redefine the array $\mathbf{d_1}$ as the difference between the existing array and the predicted one.

To be specific, we use the spline S_r that interpolates the sequence $\mathbf{e_1}$ and predict the array $\hat{\mathbf{d}}_1$. The array $\hat{\mathbf{d}}_1$, which is the DFT of $\mathbf{d_1}$, is predicted by the array $\hat{\boldsymbol{\sigma}}$ defined in (2.7) and (2.8). The DFT of the new d array is defined as follows:

$$\hat{d}_1^u(\nu) = \hat{d}_1(\nu) - \hat{e}_1(\nu)\omega_N^{\nu} U_1(\nu), \qquad \nu = 0, \ldots, m-1. \tag{3.11}$$

From now on, the superscript u means an *update* operation of the array.

Lifting: We update the even array using the new odd array

$$\hat{e}_1^u(\nu) = \hat{e}_1(\nu) + \beta_1(\nu)\omega_N^{-\nu}\hat{d}_1^u(\nu). \tag{3.12}$$

Generally, the goal of this step is to eliminate aliasing that appears while downsampling the original signal $\mathbf{x}$ into $\mathbf{e_1}$. By doing so, we have that $\mathbf{e_1}$ is transformed into a lowpass filtered and downsampled replica of $\mathbf{x}$. In Section IV-C, we will discuss how to achieve this effect by a proper choice of the control filter β_1, but for now, we only require $\beta_1(\nu)$ to be a real-valued N-periodic sequence, which obeys the condition $\beta_1(\nu + m) = -\beta_1(\nu)$.

2) Reconstruction: The reconstruction of the signal $\mathbf{x}$ from the arrays $\mathbf{e_1^u}$ and $\mathbf{d_1^u}$ is implemented in reverse order:

1) undo lifting;
2) undo predict;
3) unsplit.

Undo Lifting: We immediately restore the even array

$$\hat{e}_1(\nu) = \hat{e}_1^u(\nu) - \beta_1(\nu)\omega_N^{-\nu}\hat{d}_1^u(\nu). \tag{3.13}$$

Undo Predict: We restore the odd array

$$\hat{d}_1(\nu) = \hat{d}_1^u(\nu) + \hat{e}_1(\nu)\omega_N^{\nu} U_1(\nu), \qquad \nu = 0, \ldots, m-1. \tag{3.14}$$

Let us rewrite (3.14) using (3.13)

$$\begin{aligned}\hat{d}_1(\nu) &= \hat{d}_1^u(\nu) + \omega_N^{\nu} U_1(\nu)\left(\hat{e}_1^u(\nu) - \beta_1(\nu)\omega_N^{-\nu}\hat{d}_1^u(\nu)\right)\\ &= \hat{d}_1^u(\nu)\left(1 - \beta_1(\nu)\omega_N^{-\nu}U_1(\nu)\right) + \omega_N^{\nu}U_1(\nu)\hat{e}_1^u(\nu).\end{aligned} \tag{3.15}$$

Unsplit: The last step represents the standard restoration of the signal from its even and odd components. In the frequency domain, it looks like

$$\hat{x}(\nu) = \widehat{e_1}(\nu) + \omega_N^{-\nu}\hat{d}_1(\nu), \qquad \nu = 0, \ldots, N-1. \tag{3.16}$$

B. Dual Scheme

In the primal construction that was described above, the update step followed the prediction. In some applications, it is preferable to have the update step before prediction step and to control the prediction step. In particular, such dual scheme allows adaptive nonlinear wavelet transform [5] by choosing different predictors for different fragments of the signal. We now explain the dual scheme.

1) Decomposition:

1) We start by averaging the even array with its prediction that was derived from the odd array:
$$\hat{e}_1^u(\nu) = \tfrac{1}{2}\left(\hat{e}_1(\nu) + \omega_N^{-\nu}U_1(\nu)\hat{d}_1(\nu)\right). \tag{3.17}$$
Such an update results in a smoother even array.
2) We form the details array by extracting from the odd array the new even array supplied with the control function $\beta_1(\nu)$:
$$\hat{d}_1^u(\nu) = \hat{d}_1(\nu) - 2\beta_1(\nu)\omega_N^{\nu}\hat{e}_1^u(\nu). \tag{3.18}$$

2) Reconstruction:

1) We restore the odd array
$$\hat{d}_1(\nu) = \hat{d}_1^u(\nu) + 2\beta_1(\nu)\omega_N^{\nu}\hat{e}_1^u(\nu).$$
2) To reconstruct the even array, we use $\hat{d}_1(\nu)$:
$$\hat{e}_1(\nu) = 2\hat{e}_1^u(\nu) - \omega_N^{-\nu}U_1(\nu)\hat{d}_1(\nu).$$
3) Finally
$$\hat{x}(\nu) = \widehat{e_1}(\nu) + \omega_N^{-\nu}\hat{d}_1(\nu), \qquad \nu = 0, \ldots, N-1.$$

IV. Filterbanks and Related Bases

A. Filterbanks

Lifting schemes, which were presented above, yield efficient algorithms for the implementation of the forward and backward transform of $\mathbf{x} \longleftrightarrow \mathbf{e_1^u} \cup \mathbf{d_1^u}$, but these operations can be interpreted as transformations of the signals by a filter bank that possesses the perfect reconstruction properties.

First, we define two filter functions

$$\begin{aligned}B_{l,r}^1(\nu) &\triangleq (1 + U_1(\nu))/2\\ &= \frac{\left(\cos\frac{\nu\pi}{N}\right)^{2r}}{\left(\cos\frac{\nu\pi}{N}\right)^{2r} + \left(\sin\frac{\nu\pi}{N}\right)^{2r}}\\ &= \frac{1}{1 + \left(\tan\frac{\nu\pi}{N}\right)^{2r}}, \qquad \nu = 0, \ldots, N-1\end{aligned}$$

$$\begin{aligned}B_{h,r}^1(\nu) &\triangleq (1 - U_1(\nu))/2\\ &= \frac{\left(\sin\frac{\nu\pi}{N}\right)^{2r}}{\left(\cos\frac{\nu\pi}{N}\right)^{2r} + \left(\sin\frac{\nu\pi}{N}\right)^{2r}}\\ &= \frac{1}{1 + \left(\cot\frac{\nu\pi}{N}\right)^{2r}}, \qquad \nu = 0, \ldots, N-1.\end{aligned}$$

From (2.10), it is clear that the linear phase filter $B_{l,r}^1(\nu)$ is equal to the magnitude squared frequency-response function of the discrete-time lowpass halfband Butterworth filter of order r

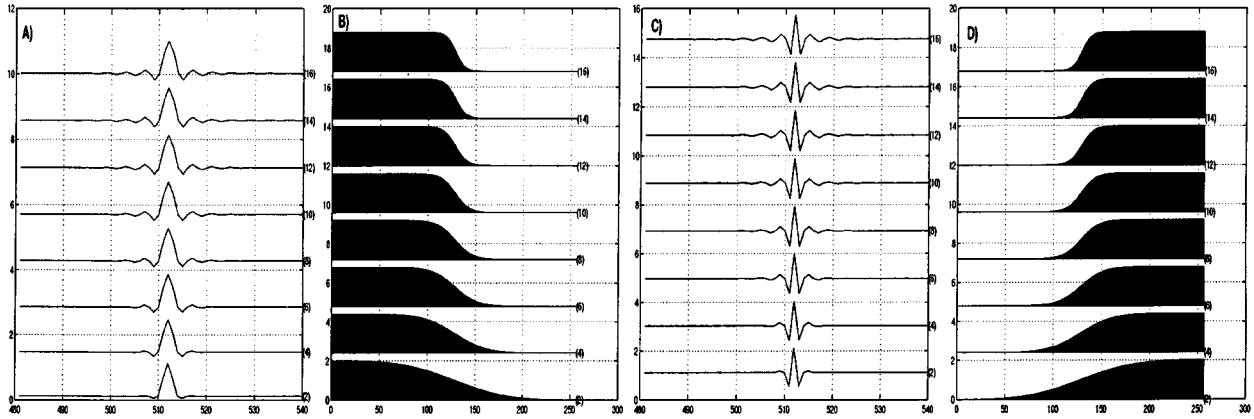

Fig. 2. (a) Low-frequency reconstruction wavelets φ^1 of order $r = 1$ at the bottom to order $r = 8$ at the top. (b) Fourier transforms of (a), which are the filters h^1. (c) High-frequency decomposition wavelets $\bar{\psi}^1$. (d) Fourier transforms of (c), which are the filters $\bar{g}^1$.

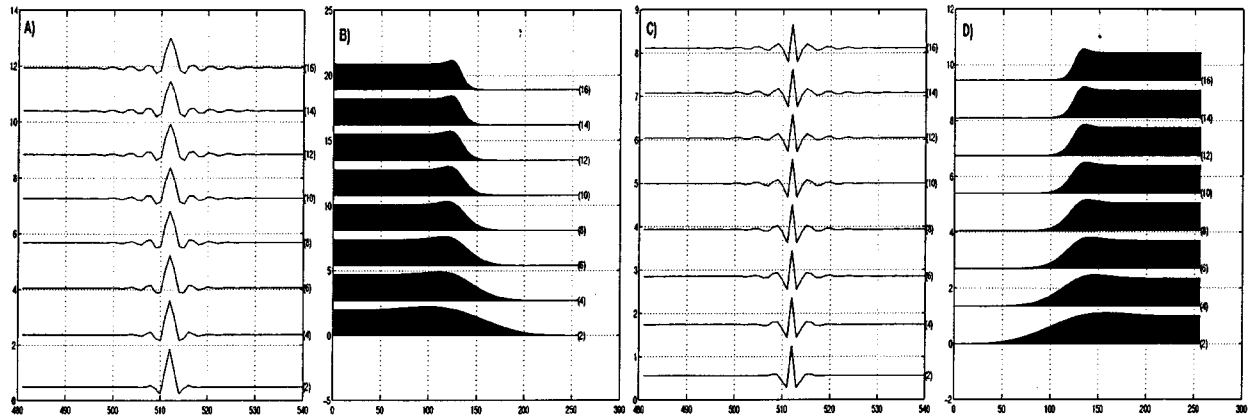

Fig. 3. (a) Low-frequency decomposition wavelets $\bar{\varphi}^1_\beta$ of order $r = 1$ at the bottom to order $r = 8$ at the top. (b) Fourier transforms of (a), which are the filters $\bar{h}^1_\beta$. (c) High-frequency reconstruction wavelets ψ^1_β. (d) Filters g^1_β for the wavelet of order r. The control filter $\beta_1(\nu) = U^1(\nu)/2$.

[12]. The linear-phase filter $B^1_{h,r}(\nu)$ is equal to the magnitude squared function of the highpass halfband Butterworth filter. It means that application of these filters on a signal is equivalent to application of two passes (forward and backward) of the corresponding Butterworth filters. We call these filters the bidirectional Butterworth filters.

Theorem 4.1: Define the N-periodic filter functions

$$\begin{aligned}\tilde{g}^1(\nu) &\triangleq 2\omega_N^{-\nu} B^1_{h,r}(\nu)\\ \tilde{h}^1_\beta(\nu) &\triangleq 1 + 2\beta_1(\nu) B^1_{h,r}(\nu)\\ &= 1 + \beta_1(\nu)\omega_N^{\nu}\tilde{g}^1(\nu) \qquad (4.19)\\ h^1(\nu) &= 2B^1_{l,r}(\nu)\\ g^1_\beta(\nu) &= 2\omega_N^{-\nu} B^1_{l,r}(\nu)\\ &= \omega_N^{-\nu}\left(1 - \beta_1(\nu)\, h^1(\nu)\right)\\ &\qquad \nu = 0, \ldots, N-1. \qquad (4.20)\end{aligned}$$

Then, the decomposition and reconstruction formulas of the primal scheme can be represented as follows:

$$\hat{e}^u_1(\nu) = \tfrac{1}{2}\left(\overline{\tilde{h}^1_\beta(\nu)}\hat{x}(\nu) + \overline{\tilde{h}^1_\beta(\nu+m)}\hat{x}(\nu+m)\right) \qquad (4.21)$$

$$\hat{d}^u_1(\nu) = \tfrac{1}{2}\left(\overline{\tilde{g}^1(\nu)}\hat{x}(\nu) + \overline{\tilde{g}^1(\nu+m)}\hat{x}(\nu+m)\right) \qquad (4.22)$$

$$\hat{x}(\nu) = h^1(\nu)\hat{e}^u_1(\nu) + g^1_\beta(\nu)\hat{d}^u_1(\nu). \qquad (4.23)$$

Proof: The proof is in the Appendix.

We call the sequences $\{\tilde{h}^1_\beta(\nu)\}$ and $\{\tilde{g}^1(\nu)\}, \nu = 0, \ldots N-1$ the frequency responses of the lowpass and high-pass decomposition of filters of the first level, respectively. We call the sequences $\{h^1(\nu)\}$ and $\{g^1_\beta(\nu)\}$ the frequency responses of the lowpass and highpass reconstruction filters of the first level, respectively. These four filter sequences form a perfect reconstruction filterbank [14]. We display the functions h^1 and $\tilde{g}^1$ in Fig. 2 and the functions $\tilde{h}^1_\beta$ and g^1_β in Fig. 3.

Theorem 4.2: With any N-periodic sequence $\beta^1(\nu)$ that satisfies the condition $\beta^1(\nu + m) = -\beta^1(\nu)$, the functions $\{\tilde{h}^1_\beta(\nu)\}$, $\{\tilde{g}^1(\nu)\}$, $\{h^1(\nu)\}$, and $\{g^1_\beta(\nu)\}$ satisfy the perfect reconstruction conditions

$$\begin{aligned} h^1(\nu)\overline{\tilde{h}^1_\beta(\nu)} + g^1_\beta(\nu)\overline{\tilde{g}^1(\nu)} &= 2\\ h^1(\nu)\overline{\tilde{h}^1_\beta(\nu+m)} + g^1_\beta(\nu)\overline{\tilde{g}^1(\nu+m)} &= 0. \qquad (4.24)\end{aligned}$$

From the definitions (4.19) and (4.20), we immediately derive

$$\begin{aligned} &h^1(\nu)\overline{\tilde{h}^1_\beta(\nu)} + g^1_\beta(\nu)\overline{\tilde{g}^1(\nu)}\\ &\quad = (1 + U_1(\nu))(1 + \beta_1(\nu)(1 - U_1(\nu)))\\ &\qquad + (1 - U_1(\nu))(1 - \beta_1(\nu)(1 + U_1(\nu))) = 2.\end{aligned}$$

The equations (4.24) can be similarly checked. ■

Similar facts hold for the dual transforms. Let us denote by $\tilde{H}^1$ and $\tilde{G}^1_\beta$ the dual decomposition filters and by H^1_β and G^1 the dual reconstruction filters. The dual decomposition filters

coincide (up to constant factors) with the reconstruction filters and vice versa, i.e.,

$$\tilde{H}^1(\nu)=h^1(\nu)/2, \qquad \tilde{G}^1_\beta(\nu)=g^1_\beta(\nu)$$
$$H^1_\beta(\nu)=2\tilde{h}^1_\beta(\nu), \qquad G^1(\nu)=\tilde{g}^1(\nu).$$

The following is an obvious observation.

Proposition 4.1: The filter functions are linked in the following way:

$$\tilde{g}^1(\nu)=\omega_N^{-\nu}h^1(\nu+m); \qquad g^1_\beta(\nu)=\omega_N^{-\nu}\overline{\tilde{h}^1_\beta(\nu+m)}.$$

Remark: We stress that the dual decomposition filter $\tilde{H}^1(\nu)$ and the primal reconstruction filter $h^1(\nu)$ are equal (up to constant factors) to the bidirectional lowpass halfband Butterworth filter of order r. The primal decomposition filter $\tilde{g}^1(\nu)$ and the dual reconstruction filter $G^1(\nu)$ multiplied by ω_N^ν are equal to the bidirectional highpass halfband Butterworth filter.

B. Bases for the Signal Space

The perfect reconstruction filter banks that were constructed above are associated with the biorthogonal pairs of bases in the space $\mathcal{S}$ of N-periodic discrete signals.

Notation:

$$\varphi^1(l)=\frac{1}{N}\sum_{\nu=0}^{N-1}e^{2\pi j\nu l/N}h^1(\nu)$$
$$\psi^1_\beta(l)=\frac{1}{N}\sum_{\nu=0}^{N-1}e^{2\pi j\nu l/N}g^1_\beta(\nu) \tag{4.25}$$
$$\tilde{\varphi}^1_\beta(l)=\frac{1}{N}\sum_{\nu=0}^{N-1}e^{2\pi j\nu l/N}\tilde{h}^1_\beta(\nu)$$
$$\tilde{\psi}^1(l)=\frac{1}{N}\sum_{\nu=0}^{N-1}e^{2\pi j\nu l/N}\tilde{g}^1(\nu). \tag{4.26}$$

Definition 4.1: The functions φ^1 and ψ^1_β given by (4.25), which belong to the space $\mathcal{S}$, are called the low-frequency and high-frequency reconstruction wavelets of the first scale, respectively. The functions $\tilde{\varphi}^1_\beta$ and $\tilde{\psi}^1$ given by (4.26), which belong to the space $\mathcal{S}$, are called the low-frequency and high-frequency decomposition wavelets of the first scale, respectively.

Note that the wavelets in (4.25) and (4.26) are the IDFT of the corresponding filters.

Theorem 4.3: The shifts of wavelets defined by (4.25) and (4.26) form a biorthogonal pairs of bases in the space $\mathcal{S}$. This means that any signal $\mathbf{x}\in\mathcal{S}$ can be represented as

$$x(l)=\sum_{k=0}^{m-1}e^u_1(k)\varphi^1(l-2k)+\sum_{k=0}^{m-1}d^u_1\psi^1_\beta(l-2k).$$

The coordinates $e^u_1(k)$ and $d^u_1(k)$ are the IDFT of the arrays $\hat{e}^u_1(k)$ and $\hat{d}^u_1(k)$, respectively. They can be represented as inner products

$$e^u_1(k)=\left\langle \mathbf{x},\, \tilde{\varphi}^1_{\beta,\,k}\right\rangle, \quad \text{where } \tilde{\varphi}^1_{\beta,\,k}(l)=\tilde{\varphi}^1_\beta(l-2k) \tag{4.27}$$
$$d^u_1(k)=\left\langle x^{\nu+1},\, \tilde{\psi}^1_k\right\rangle, \quad \text{where } \tilde{\psi}^1_k(l)=\tilde{\psi}^1(l-2k). \tag{4.28}$$

Proof: The proof is in the Appendix.

Corollary 4.1: The following biorthogonal relations hold:

$$\left\langle \tilde{\varphi}^1_{\beta,\,k},\, \varphi^1_l\right\rangle=\left\langle \psi^1_{\beta,\,k},\, \tilde{\psi}^1_l\right\rangle=\delta^l_k,$$
$$\left\langle \tilde{\varphi}^1_{\beta,\,k},\, \psi^1_{\beta,\,l}\right\rangle=\left\langle \tilde{\psi}^1_l,\, \varphi^1_k\right\rangle=0, \qquad \forall l,\, k.$$

Remark: The decomposition wavelets of the dual scheme are the reconstruction wavelets for the primal scheme and vice versa.

C. Choosing the Control Filter

Thus far, we did not specify the filter sequence $\beta_1(\nu)$, which occurs during construction of the primal filters $g^1_\beta(\nu)$ and $\tilde{h}^1_\beta(\nu)$ and the dual ones $\tilde{G}^1_\beta(\nu)$ and $H^1_\beta(\nu)$. The only imposed requirement was $\beta^1(\nu+m)=-\beta^1(\nu)$. Therefore, we are free to use this function β_1 for custom design of these filters and the corresponding wavelets. We present two possible approaches for choosing the control filter $\beta_1(\nu)$.

1) Retaining the Maximal Flatness of the Filters: As was mentioned above, the dual decomposition filter $\tilde{H}^1(\nu)$ [the primal reconstruction filter $h^1(\nu)$] and the primal decomposition filter $\tilde{g}^1(\nu)$ [the dual reconstruction filter $G^1(\nu)$] multiplied by ω_N^ν are equal to the bidirectional lowpass and highpass halfband Butterworth filters of order r, respectively. These filters are linear phase and maximally flat in their passband and stopband due to the factors $(\cos(\nu\pi/N))^{2r}$ for the lowpass filters and $(\sin(\nu\pi/N))^{2r}$ for the highpass filters. In Fig. 2, we display these filters and the wavelets φ^1 and $\tilde{\psi}^1$, which are related to them. We will retain similar properties for filters that depend on β_1.

An easy way to achieve this is to put

$$\begin{aligned}\beta_1(\nu)&=\beta^1_1(\nu)\\&=U_1(\nu)/2\\&=\frac{1}{2}\,\frac{\left(\cos\frac{\nu\pi}{N}\right)^{2r}-\left(\sin\frac{\nu\pi}{N}\right)^{2r}}{\left(\cos\frac{\nu\pi}{N}\right)^{2r}+\left(\sin\frac{\nu\pi}{N}\right)^{2r}}.\end{aligned} \tag{4.29}$$

Then, we have

$$\begin{aligned}\tilde{h}^1_\beta(\nu)&=1+\tfrac{1}{2}U_1(\nu)(1-U_1(\nu))\\&=\tfrac{1}{2}[(1+U_1(\nu))+(1+U_1(\nu))(1-U_1(\nu))]\\&=B^1_{l,\,r}(\nu)+2B^1_{l,\,r}(\nu)B^1_{h,\,r}(\nu)\\&=B^1_{l,\,r}(\nu)(1+2B^1_{h,\,r}(\nu)).\end{aligned} \tag{4.30}$$

Similarly

$$\begin{aligned}g^1_\beta(\nu)&=\omega_N^{-\nu}\left(1-\tfrac{1}{2}U_1(\nu)(1+U_1(\nu))\right)\\&=\omega_N^{-\nu}\left[B^1_{h,\,r}(\nu)+2B^1_{l,\,r}(\nu)B^1_{h,\,r}(\nu)\right]\\&=\omega_N^{-\nu}\left[B^1_{h,\,r}(\nu)(1+2B^1_{l,\,r}(\nu))\right].\end{aligned} \tag{4.31}$$

We conclude from (4.30) and (4.31) that, as in the case of the filters $h^1(\nu)$ and $\tilde{g}^1(\nu)$, the filters $\tilde{h}^1_\beta(\nu)$ and $g^1_\beta(\nu)$ are also the mirrored replicas of each other. They differ from bidirectional Butterworth filters of order r by the term $\gamma^1_1=2B^1_{l,\,r}(\nu)B^1_{h,\,r}(\nu)$, which affects only the central part of the frequency domain. We display these filters and the

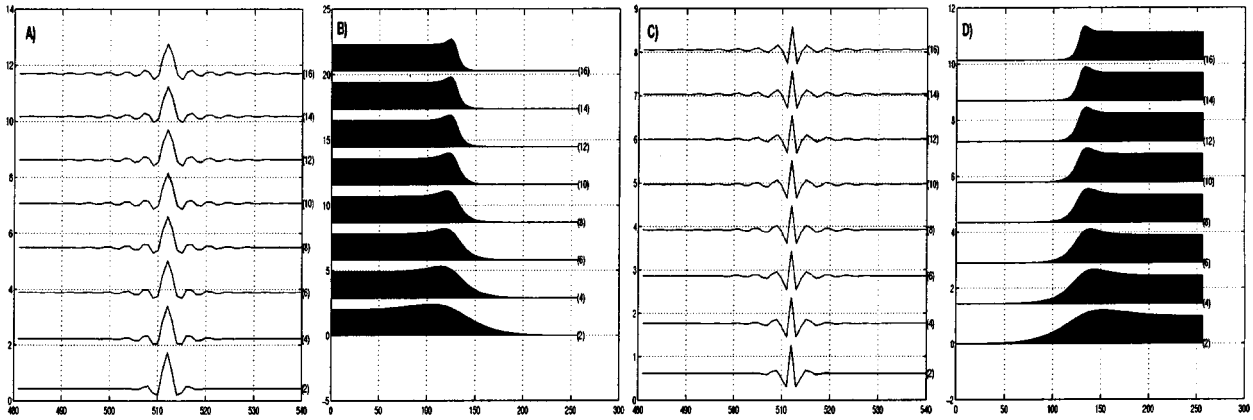

Fig. 4. (a) Low-frequency decomposition wavelets $\bar{\varphi}_b^1$ of order $r = 1$ at the bottom to order $r = 8$ at the top. (b) Fourier transforms of (a), which are the filters $\tilde{h}_b^1$. (c) High-frequency reconstruction wavelets ψ_b^1. (d) Filters g_b^1 for the wavelet of order r. The control filter $\beta_1(\nu) = U^1(\nu)/(1 + (U^1(\nu)^2)$.

corresponding wavelets in Fig. 3. We observe that the filters and the wavelets are similar to the previous ones but the flatness of the filters is disturbed by the bumps ("over shooting") near the cutoff. These bumps appear due to the term γ_1^1. For higher r, we get sharper cutoff, and the "overshooting" becomes more visible.

2) Orthogonality of the Wavelets: Another suggestion for the choice of β is triggered by the following consideration. Generally, the high- and low-frequency wavelets $\varphi^1(l)$ and $\psi_\beta^1(l)$, respectively, are not orthogonal to each other, and neither are $\tilde{\varphi}_\beta^1(l)$ and $\tilde{\psi}^1(l)$. However, by proper choice of the control filter $\beta_1(\nu)$, we can get this property. In this case, the signals $\mathbf{x}_h$ and $\mathbf{x}_g$, in the representation $\mathbf{x} = \mathbf{x}_h + \mathbf{x}_g$, become orthogonal to each other. By this means, we are able to remarkably reduce the redundancy that is inherent to the biorthogonal wavelet transforms. Moreover, the decomposition wavelets $\tilde{\varphi}_{\beta,\,k}^1$ belong to the same subspace to which the reconstruction wavelets φ_l^1 belong. The wavelets $\tilde{\varphi}_{\beta,\,k}^1$ can be expressed as linear combinations of the wavelets φ_l^1 and vice versa. The same is true for the highpass wavelets $\tilde{\psi}_k^1$ and $\psi_{\beta,\,l}^1$.

Proposition 4.2: If the control filter $\beta^1(\nu)$ is chosen as

$$\begin{aligned}\beta_1(\nu) &= \beta_1^2(\nu) \\ &= \frac{U_1(\nu)}{1 + (U_1(\nu))^2} \\ &= \frac{1}{2}\,\frac{\left(\cos\dfrac{\nu\pi}{N}\right)^{4r} - \left(\sin\dfrac{\nu\pi}{N}\right)^{4r}}{\left(\cos\dfrac{\nu\pi}{N}\right)^{4r} + \left(\sin\dfrac{\nu\pi}{N}\right)^{4r}}\end{aligned} \tag{4.32}$$

then the following orthogonal relations hold:

$$\left\langle \psi_{\beta,\,k}^1,\, \varphi_l^1 \right\rangle = \left\langle \tilde{\varphi}_{\beta,\,k}^1,\, \tilde{\psi}_l^1 \right\rangle = 0, \qquad \forall\, l,\, k. \tag{4.33}$$

Remark: When we doubled the order of the filer $\beta_1^1(\nu)$, which is given by (4.29), we get the filter $\beta_1^2(\nu)$.

Proof: The proof is in the Appendix.

When the control function $\beta_1(\nu) = \beta_1^2(\nu)$, then the lowpass filter is

$$\begin{aligned}\tilde{h}_\beta^1(\nu) &= \frac{\left(\cos\dfrac{\nu\pi}{N}\right)^{2r}\left(\left(\cos\dfrac{\nu\pi}{N}\right)^{2r} + \left(\sin\dfrac{\nu\pi}{N}\right)^{2r}\right)}{\left(\cos\dfrac{\nu\pi}{N}\right)^{4r} + \left(\sin\dfrac{\nu\pi}{N}\right)^{4r}} \\ &= B_{l,\,2r}(\nu) + \gamma_1^2(\nu)\end{aligned}$$

and the highpass filter is

$$\begin{aligned}g_\beta^1(\nu) &= \omega_N^{-\nu}\,\frac{\left(\sin\dfrac{\nu\pi}{N}\right)^{2r}\left(\left(\cos\dfrac{\nu\pi}{N}\right)^{2r} + \left(\sin\dfrac{\nu\pi}{N}\right)^{2r}\right)}{\left(\cos\dfrac{\nu\pi}{N}\right)^{4r} + \left(\sin\dfrac{\nu\pi}{N}\right)^{4r}} \\ &= \omega_N^{-\nu}\left(B_{h,\,2r}(\nu) + \gamma_1^2(\nu)\right),\end{aligned}$$

where

$$\gamma_1^2(\nu) \triangleq \frac{\left(\cos\dfrac{\nu\pi}{N}\right)^{2r}\left(\sin\dfrac{\nu\pi}{N}\right)^{2r}}{\left(\cos\dfrac{\nu\pi}{N}\right)^{4r} + \left(\sin\dfrac{\nu\pi}{N}\right)^{4r}}.$$

We see that in this case, the filters coincide with the bidirectional Butterworth filters of order $2r$ up to the term $\gamma_1^2(\nu)$. The filter $\gamma_1^2(\nu)$ is similar to the filter $\gamma_1^1(\nu)$), which appeared when we choose $\beta_1(\nu) = \beta_1^1(\nu)$. We display the filters and the corresponding wavelets in Fig. 4. We observe that the filters and the wavelets resemble the filters and wavelets with $\beta_1(\nu) = U^1(\nu)/2$, but now, the bumps are more visible, and the cutoffs are steeper than before. The wavelets are somewhat smoother but fail in spatial localization.

All the filters that are used in our wavelet transform are either a combination of the bidirectional Butterworth filters or are very close to it. Therefore, it is appropriate to name the corresponding wavelets the *biorthogonal Butterworth wavelets*.

Remark: Note that the decomposition highpass filters of order r comprise the factor $(\sin(\nu\pi/N))^{2r}$. In the time domain, this factor corresponds to a finite difference of order $2r$. It means that if a fragment of the signal $\mathbf{x}$ coincides (or is near to) a polynomial of degree $2r - 1$, then the coefficients $d^u(k)$ are related to this fragment are equal (or near) to zero. This property is the periodic substitution of the property of vanishing moments.

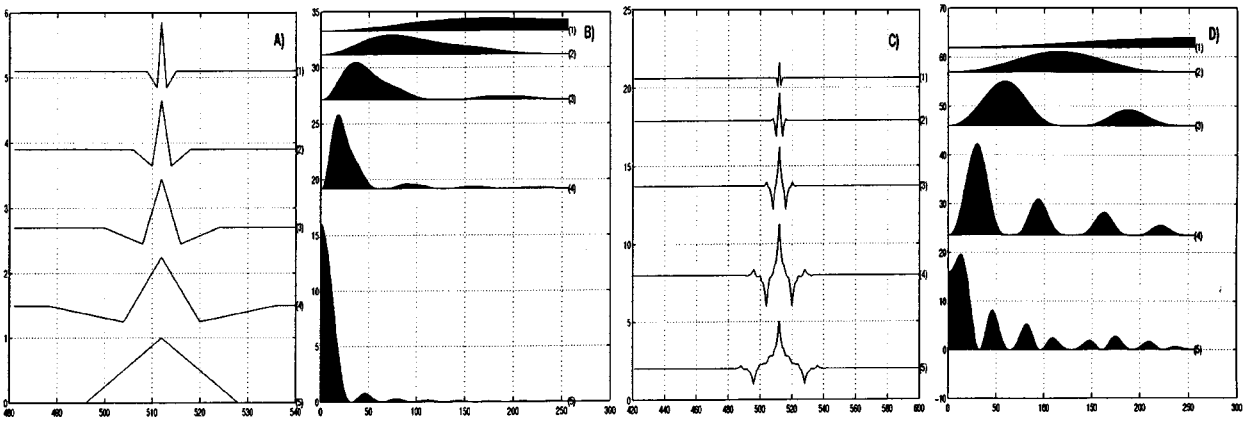

Fig. 5. (a) Reconstruction wavelets ψ^l_β, $l = 1 \cdots 4$ of order 1 (lines 1–4) and φ^l, $l = 4$ (line 5). (b) Their spectra. (c) Decomposition wavelets $\bar{\psi}^l_\beta$, $l = 1 \cdots 4$ of order 1 (lines 1–4), and $\bar{\varphi}^l_\beta$, $l = 4$ (line 5). (d) Their spectra.

V. Multiscale Wavelet Transforms

Repeated applications of the transform can be achieved in an iterative way. It can be implemented as either a linear invertible transform of a wavelet type or as a wavelet packet type transform, which results in an overcomplete representation of the signal. In this section, we explain one multiscale advance of the wavelet transform.

In this transform, we store the array $\mathbf{d}^u_1$ and decompose the array $\mathbf{e}^u_1$. Actually, we have at our disposal the DFT arrays $\hat{\mathbf{e}}^u_1$ and $\hat{\mathbf{d}}^u_1$ that were derived in the previous step [see (3.11) and (3.12) or (3.17) and (3.18)]. The IDFT is applied on the array $\hat{\mathbf{d}}^u_1$ that yields $\mathbf{d}^u_1$.

Let $\mathbf{e}^u_2$ and $\mathbf{d}^u_2$ denote the even and odd subarrays of the array $\mathbf{e}^u_1$. We can find the values of the corresponding DFT directly from $\hat{\mathbf{e}}^u_1$:

$$\begin{aligned}\hat{e}_2(\nu) &= \left(\hat{e}^u_1(\nu) + \hat{e}^u_1(\nu + m/2)\right)/2\\ \hat{d}_2(\nu) &= \omega^{\nu}_{N/2}\left(\hat{e}^u_1(\nu) - \hat{e}^u_1(\nu + m/2)\right)/2.\end{aligned}$$

The filters for the first step of the transform were produced from the function U_1 [see (2.8)]. We produce the filters for the second step using the new function U_2, which is the downsampled version of U_1: $U_2(\nu) = U_1(2\nu)$ [see (2.8)].

The decomposition steps for the primal scheme are the following.

1) $\hat{d}^u_2(\nu) = \hat{d}_2(\nu) - \omega^{\nu}_{N/2}\hat{e}_2(\nu)U_2(\nu)$.
2) $\hat{e}^u_2(\nu) = \hat{e}_2(\nu) + \beta^2(\nu)w^{-\nu}_{N/2}\hat{d}^u_2(\nu)$.
3) The array $\mathbf{d}^u_2$ is derived by the application of the IDFT. If we terminate the decomposition at this step, we apply IDFT on $\hat{\mathbf{e}}^u_2$ as well and produce $\mathbf{e}^u_2$. In this case, the original array $\mathbf{x}$ is transformed into the array $\{\mathbf{d}^u_1, \mathbf{d}^u_2, \mathbf{e}^u_2\}$. To proceed in getting coarser scales in the decomposition, we use the array $\hat{\mathbf{e}}^u_2$ rather than $\mathbf{e}^u_2$.

The reconstruction steps are the following.

1) Apply the DFT on $\mathbf{d}^u_2$. If $\hat{\mathbf{e}}^u_2$ is not available from the previous steps of the reconstruction, apply it on $\mathbf{e}^u_2$.
2) $\hat{e}_2(\nu) = \hat{e}^u_2(\nu) - \beta^2(\nu)w^{-\nu}_{N/2}\hat{d}^u_2(\nu)$.
3) $\hat{d}_2(\nu) = \hat{d}^u_2(\nu) + \omega^{\nu}_{N/2}\hat{e}_2(\nu)U_2(\nu)$.
4) $\hat{e}_2(\nu) = \hat{e}_2(\nu) + \omega^{-\nu}_{N/2}\hat{d}_2(\nu)$.

The dual scheme is implemented in a similar manner.

The described transform is linked with the $N/2$-periodic filters $\tilde{g}^2(\nu)$, $\tilde{h}^2_\beta(\nu)$, $h^2(\nu)$, and $g^2_\beta(\nu)$, which are the downsampled versions of the corresponding filters of the first step. It is worth noting that the filters $\tilde{g}^2(\nu)$ and $h^2(\nu)$ are bidirectional Butterworth filters. The filters $\tilde{h}^2_\beta$ and $\tilde{g}^2$ are applied on the array $\hat{\mathbf{e}}^u_1$ to derive $\hat{\mathbf{e}}^u_2$ and $\hat{\mathbf{d}}^u_2$. Conversely, h^2 and g^2_β are applied on the arrays $\hat{\mathbf{e}}^u_2$ and $\hat{\mathbf{d}}^u_2$ to restore $\hat{\mathbf{e}}^u_1$.

The transform can be viewed as an expansion of the signal with biorthogonal pair of bases:

$$\begin{aligned}x(l) = &\sum_{k=0}^{m/2-1} e^u_2(k)\varphi^2(l-4k)\\ &+ \sum_{k=0}^{m/2-1} d^u_2(k)\psi^2_\beta(l-4k)\\ &+ \sum_{k=0}^{m-1} d^u_1(k)\psi^1_\beta(l-2k) \qquad (5.34)\end{aligned}$$

where lowpass and highpass reconstruction wavelets of the second scale are defined as

$$\begin{aligned}\varphi^2(l) &= \frac{1}{N}\sum_{\nu=0}^{N-1} e^{2\pi j\nu l/N}h^1(\nu)h^2(\nu)\\ \psi^2_\beta(l) &= \frac{1}{N}\sum_{\nu=0}^{N-1} e^{2\pi j\nu l/N}h^1(\nu)g^2_\beta(\nu).\end{aligned}$$

The coordinates in (5.34) are inner products with four-sample shifts of the decomposition wavelets of the second scale

$$\begin{aligned}\tilde{\varphi}^2_\beta(l) &= \frac{1}{N}\sum_{\nu=0}^{N-1} e^{2\pi j\nu l/N}\tilde{h}^1_\beta(\nu)\tilde{h}^2_\beta(\nu)\\ \tilde{\psi}^2_\beta(l) &= \frac{1}{N}\sum_{\nu=0}^{N-1} e^{2\pi j\nu l/N}\tilde{h}^1_\beta(\nu)\tilde{g}^2(\nu).\end{aligned}$$

In Fig. 5, we display the biorthogonal Butterworth wavelets of order 1 up to the fourth level and their spectra. Note that these wavelets are compactly supported and have two vanishing moments. In Fig. 6, we display wavelets of order 10 up to the fourth level and their spectra. These wavelets were outperformed by

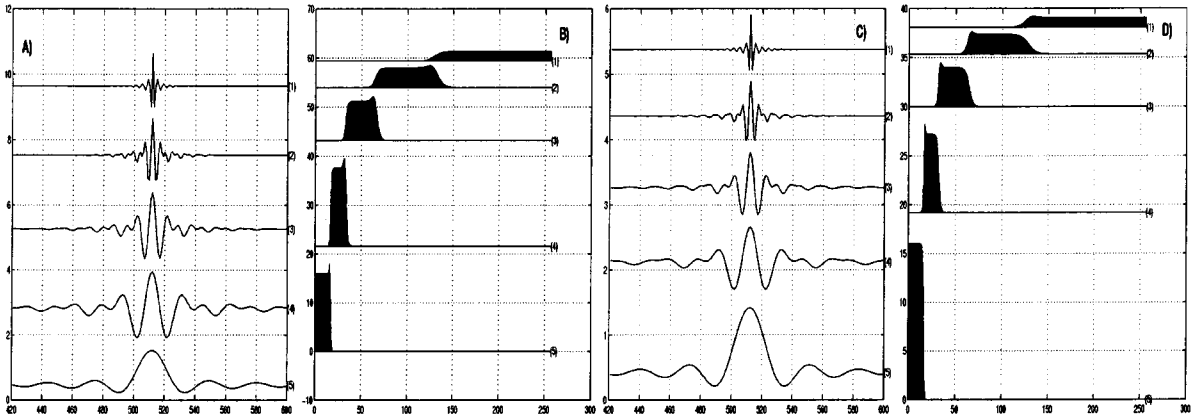

Fig. 6. (a) Reconstruction wavelets ψ_β^l, $l = 1 \cdots 4$ of order 10 (lines 1–4) and φ^l, $l = 4$ (line 5). (b) Their spectra. (c) Decomposition wavelets $\bar{\psi}_\beta^l$, $l = 1 \cdots 4$ of order 1 (lines 1–4), and $\bar{\varphi}_\beta^l$, $l = 4$ (line 5). (d) Their spectra.

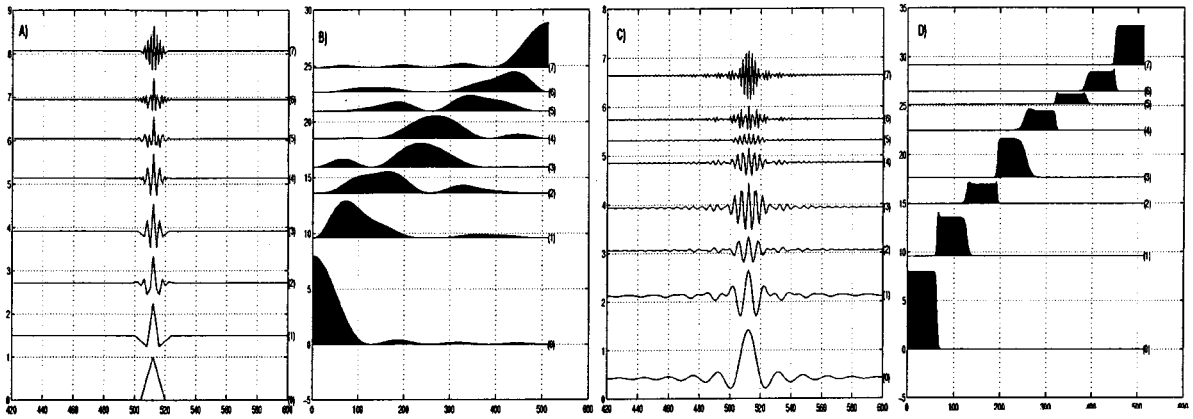

Fig. 7. (a) Wavelet packets of third scale of order 1 (compactly supported). (b) Their spectra. (c) Wavelet packets of third scale of order 15. (d) Their spectra.

the wavelets of lower orders in spatial localization but win in frequency localization and smoothness.

Unlike the mechanism in the wavelet transform, in the wavelet packet transform, both subarrays $\mathbf{e}_1^u$ and $\mathbf{d}_1^u$ of the first scale are subject to decomposition that produces four second-scale subarrays. In turn, these four arrays produce eight subarrays for the third scale, and so on. All subarrays that are related to a certain scale are stored. Without going into details, we display in Fig. 7 the wavelet packets of the third scale of first and 15th orders and their spectra. The wavelet packets are derived by the primal transforms.

VI. Conclusions

We presented a new family of biorthogonal wavelet transforms and a related library of biorthogonal periodic symmetric waveforms. For the construction, we used the interpolatory discrete splines, which enabled us to design a library of perfect reconstruction filterbanks. These filterbanks are intimately related to Butterworth filters.

The construction is performed in a "lifting" manner that allows more efficient implementation and provides tools for custom design of the filters and wavelets. As it is common in lifting schemes, the computations can be carried out "in place," and the inverse transform is performed in a reverse order. The difference with the conventional lifting scheme [16] is that all the transforms are implemented in the frequency domain with the use of the fast Fourier transform (FFT). However, the time-domain implementation is possible by means of recursive IIR filtering similar to the implementation of the digital Butterworth filters.

We suggested two ways to choose the control filters that are inherent in the transforms. However, many more ways are possible. This subject deserves a special investigation.

High-frequency filters of an order r in our construction comprise the factor $(\sin(\nu\pi/N))^{2r}$. In a nonperiodic setting, it corresponds to the vanishing moments property up to order $2r$ of the corresponding wavelets. Thus, such a filter turns fragments of the signal, which (almost) coincide with polynomial of degree p, close to zero. The low-frequency filters, on the contrary, leave the fragments almost intact.

Our algorithm allows a stable construction of filters comprising these sine blocks of practically any order.

The computational complexity of the application of the wavelet transform on a signal of length N is the same as the application of the FFT on a signal, which is $O(N \log_2 N)$. Increase of the order in our scheme does not affect the cost of the implementation. Therefore, especially for higher orders r, the complexity of our algorithm is comparable if not less than the complexity of the standard wavelet transform.

We should particularly emphasize that our scheme is based on interpolation, and as such, it involves only samples of signals,

and it does not require any use of quadrature formulas. This property is valuable for digital signal and image processing.

The fact that these filters have linear phase property and the basic waveforms are symmetric is also of great importance to these applications. In addition, these filters yield refined frequency resolution.

We anticipate a wide range of applications for the presented library of waveforms in signal and image processing.

APPENDIX

Proof of Theorem 4.1: We start with the primal decomposition formula (4.22). We modify (3.11) using the identities

$$\begin{aligned}\hat{e}_1(\nu) &= \tfrac{1}{2}(\hat{x}(\nu)+\hat{x}(\nu+m))\\ \hat{d}_1(\nu) &= \frac{\omega_N^{\nu}}{x}(\nu)-\hat{x}(\nu+m)).\end{aligned} \tag{7.35}$$

Therefore, we have

$$\begin{aligned}\hat{d}_1^u(\nu) &= \frac{\omega_N^{\nu}}{2}(\hat{x}(\nu)-\hat{x}(\nu+m)-U_1(\nu)(\hat{x}(\nu)+\hat{x}(\nu+m)))\\ &= \frac{\omega_N^{\nu}}{2}(\hat{x}(\nu)(1-U_1(\nu))-\hat{x}(\nu+m)(1+U_1(\nu))).\end{aligned} \tag{7.36}$$

To obtain (4.22), it is sufficient to note that the function $\tilde{g}^1$, which is defined in (4.19), possesses the property $\tilde{g}^1(\nu+m) = -\omega_N^{\nu}(1+U_1(\nu))$. Thus, we see that (7.36) is equivalent to (4.22).

To prove (4.21), we use the identity (7.35) and the already-proved relation (4.22). Moreover, we recall that $\omega_N^{-(\nu+m)}\beta_1(\nu+m) = \omega_N^{-\nu}\beta_1(\nu)$. Then, the decomposition formula (3.12) can be rewritten as

$$\begin{aligned}\hat{e}_1^u(\nu) &= \frac{1}{2}(\hat{x}(\nu)+\hat{x}(\nu+m))+\frac{\beta_1(\nu)\omega_N^{-\nu}}{2}\\ &\quad\cdot\left(\overline{\tilde{g}^1(\nu)}\hat{x}(\nu)+\overline{\tilde{g}^1(\nu+m)}\hat{x}(\nu+m)\right)\\ &= \tfrac{1}{2}\Big(\hat{x}(\nu)\left(1+\beta_1(\nu)\omega_N^{-\nu}\overline{\tilde{g}^1(\nu)}\right)+\hat{x}(\nu+m)\\ &\quad\cdot\left(1+\beta_1(\nu+m)\omega_N^{-(\nu+m)}\overline{\tilde{g}^1(\nu+m)}\right)\Big).\end{aligned}$$

Hence, (4.21) follows.

To verify the reconstruction formula (4.23), we substitute (3.13) and (3.15) into (3.16). ∎

Proof of Theorem 4.3: We start with the reconstruction formula (4.23), which we rewrite as

$$\hat{x}(\nu) = \hat{x}_h(\nu)+\hat{x}_g(\nu)$$

where

$$\hat{x}_h(\nu) = h^1(\nu)\hat{e}_1^u(\nu) \quad \text{and} \quad \hat{x}_g(\nu) = g_\beta^1(\nu)\hat{d}_1^u(\nu).$$

We have from (4.25)

$$\begin{aligned}x_h(l) &= \frac{1}{N}\sum_{\nu=0}^{N-1} e^{2\pi j\nu l/N}h^1(\nu)\sum_{k=0}^{m-1} e^{-2\pi j\nu k/m}e_1^u(k)\\ &= \sum_{k=0}^{m-1} e_1^u(k)\frac{1}{N}\sum_{\nu=0}^{N-1} e^{2\pi j\nu(l-2k)/N}h^1(\nu)\\ &= \sum_{k=0}^{m-1} e_1^u(k)\varphi^1(l-2k).\end{aligned}$$

Similarly, we derive the relation as [see (4.25)]

$$x_g(l) = \sum_{k=0}^{m-1} d_1^u\psi_\beta^1(l-2k).$$

Let us consider the decomposition formula (4.21). The property (2.1) implies that by using the IDFT, we get

$$a(k) \triangleq \frac{1}{N}\sum_{\nu=0}^{N-1} e^{2\pi j\nu k/N}\overline{\tilde{h}_\beta^1(\nu)}\hat{x}(\nu) = \sum_{l=0}^{N-1}\tilde{\varphi}_\beta^1(l-k)x(l).$$

Now, from (4.21) and (2.2), we have

$$e_1^u(k) = a(2k) = \sum_{l=0}^{N-1}\tilde{\varphi}_\beta^1(l-2k)x(l) = \langle \mathbf{x},\, \tilde{\varphi}_{\beta,\,k}^1\rangle$$

which proves (4.27). Similarly, (4.28) is proved. ∎

Proof of Proposition 4.2: Using (4.25), we can write

$$\begin{aligned}\langle\psi_{\beta,\,k}^1,\,\varphi_l^1\rangle &= \frac{1}{N^2}\sum_{n=0}^{N-1}\sum_{\nu=0}^{N-1} e^{-(2\pi j\nu(n-2l)/N)}\overline{h^1(\nu)}\\ &\quad\cdot\sum_{s=0}^{N-1} e^{2\pi js(n-2k)/N}g_\beta^1(s)\\ &= \frac{1}{N^2}\sum_{\nu,\,s=0}^{N-1}\overline{h^1(\nu)}\,g_\beta^1(s)e^{2\pi j2(ks-\nu l)/N}\\ &\quad\cdot\sum_{n=0}^{N-1} e^{-(2\pi n(s-\nu)/N)}\\ &= \frac{1}{N}\sum_{\nu=0}^{N-1}\overline{h^1(\nu)}g_\beta^1(\nu)\omega_m^{\nu(k-l)}.\end{aligned}$$

Since the function $\omega_m^{\nu(k-l)}$ is m-periodic with respect to ν, we represent the inner product as

$$\begin{aligned}&\langle\psi_{\beta,\,k}^1,\,\varphi_l^1\rangle\\ &\quad= \sum_{\nu=0}^{m-1}\omega_m^{\nu(k-l)}\left(\overline{h^1(\nu)}g_\beta^1(\nu)+\overline{h}^1(\nu+m)g_\beta^1(\nu+m)\right).\end{aligned}$$

Equations (4.19) imply that

$$\begin{aligned}&\overline{h^1(\nu)}g_\beta^1(\nu)\\ &\quad= \omega_m^{-\nu/2}((1+U_1(\nu))(1-\beta^1(\nu)(1+U_1(\nu)))\\ &\overline{h^1(\nu+m)}g_\beta^1(\nu+m)\\ &\quad= -\omega_m^{-\nu/2}((1-U_1(\nu))(1+\beta^1(\nu)(1-U_1(\nu))).\end{aligned}$$

Hence, we have

$$\begin{aligned}&\langle\psi_{\beta,\,k}^1,\,\varphi_l^1\rangle\\ &\quad= \sum_{\nu=0}^{m-1}\omega_m^{\nu(k-l-1/2)}\left(2U_1(\nu)-2\beta^1(\nu)(1+(U_1(\nu))^2)\right).\end{aligned}$$

Substitution of (4.32) results in $\langle\psi_{\beta,\,k}^1,\,\varphi_l^1\rangle = 0$. The second relation in (4.33) is similarly proved. ∎

REFERENCES

[1] T. Aboulnasr, "A mixed Butterworth/Daubechies wavelet analysis/synthesis system," in *Proc. IEEE Int. Symp. Circuits Syst.*, vol. 2, 1994, pp. 453–456.

[2] A. Aldroubi, M. Eden, and M. Unser, "Discrete spline filters for multiresolutions and wavelets of l_2," *SIAM J. Math. Anal.*, vol. 25, pp. 1412–1432, 1994.

[3] G. Battle, "A block spin construction of ondelettes—Part I. Lemarié functions," *Comm. Math. Phys.*, vol. 110, pp. 601–615, 1987.

[4] C. K. Chui and J. Z. Wang, "On compactly supported spline wavelets and a duality principle," *Trans. Amer. Math. Soc.*, vol. 330, pp. 903–915, 1992.

[5] R. L. Claypoole, Jr., J. M. Davis, W. Sweldens, and R. Baraniuk, "Nonlinear wavelet transforms for image coding via lifting," *IEEE Trans. Signal Processing*, submitted for publication.

[6] A. Cohen, I. Daubechies, and J.-C. Feauveau, "Biorthogonal bases of compactly supported wavelets," *Commun. Pure Appl. Math.*, vol. 45, pp. 485–560, 1992.

[7] D. L. Donoho, Interpolating Wavelet Transform. Stanford, CA: Preprint 408, Dept. Stat., Stanford Univ., 1992, to be published.

[8] C. Herley and M. Vetterli, "Wavelets and recursive filter banks," *IEEE Trans. Signal Processing*, vol. 41, pp. 2536–2556, Aug. 1993.

[9] P. G. Lemarié, "Ondelettes à localization exponentielle," *J. Math. Pures Appl.*, vol. 67, pp. 227–236, 1988.

[10] V. N. Malozemov, A. B. Pevnyi, and A. A. Tretyakov, "A fast wavelet transform for discrete periodic signals and images," *Probl. Inform. Transm.*, vol. 34, no. 2, pp. 161–168, 1998.

[11] V. N. Malozemov and A. B. Pevnyi, "Discrete periodic splines and their numerical application," *Comput. Math. Math. Phys.*, vol. 38, pp. 1181–1192, 1998.

[12] A. V. Oppenheim and R. W. Shafer, *Digital Signal Processing*. Englewood Cliffs, NJ: Prentice-Hall, 1989.

[13] A. B. Pevnyi and V. A. Zheludev, "On wavelet analysis in the discrete splines space," in *Proc. Second Int. Conf. Tools Math. Modeling*. St. Petersburg, Russia: St. Petersburg Tech. Univ., 1999, vol. 4, pp. 181–195.

[14] G. Strang and T. Nguen, *Wavelets and Filter Banks*. Wellesley, MA: Wellesley-Cambridge Press, 1996.

[15] I. W. Selesnick, "Formulas for orthogonal IIR wavelet filters," *IEEE Trans. Signal Processing*, vol. 46, pp. 1138–1141, Apr. 1998.

[16] W. Sweldens, "The lifting scheme: A custom design construction of biorthogonal wavelets," *Appl. Comput. Harmon. Anal.*, vol. 3, no. 2, pp. 186–200, 1996.

[17] T. E. Tuncer and G. V. H. Sandri, "Butterworth wavelets and adaptive echo cancellation," in *Proc. IEEE-SP Int. Symp. Time-Freq. Time-Scale Anal.*, 1992, pp. 451–454.

[18] V. A. Zheludev, "Periodic splines, harmonic analysis, and wavelets in 'Signal and Image Representation in Combined Spaces'," in *Wavelet Analysis and Applications*, Y. Y. Zeevi and R. Coifman, Eds. San Diego, CA: Academic, 1998, vol. 7, pp. 477–509.

[19] V. A. Zheludev and A. Z. Averbuch, "A biorthogonal waveletscheme based on interpolatory splines," in *Proc. Second Int. Conf. Tools Math. Modeling*. St. Petersburg, Russia: St. Petersburg Tech. Univ., 1999, vol. 4, pp. 214–231.

Amir Z. Averbuch was born in Tel-Aviv, Israel. He received the B.Sc. and M.Sc. degrees in mathematics from the Hebrew University, Jerusalem, Israel in 1971 and 1975, respectively, and the Ph.D. degree in computer science from Columbia University, New York, NY, in 1983.

From 1967 to 1971 and from 1973 to 1976, he served in the Israeli Defense Forces. From 1976 to 1986, he was a research staff member with the Department of Computer Science, IBM T. J. Watson Research Center, Yorktown Heights, NY. In 1987, he joined the Department of Computer Science, School of Mathematical Sciences, Tel-Aviv University, and since 1995, he has been an Associate Professor. His research interests include wavelet applications for signal/image processing and numerical computation, parallel processing and supercomputing (software and algorithms), and fast algorithms.

Alexander B. Pevnyi received the M.S. and Ph.D. degrees from St. Petersburg University, St. Petersburg, Russia, in 1970 and 1973, respectively.

From 1973 to 1975, he was an Assistant Professor with Syktyvkar University, Syktyvkar, Russia. Since 1975, he has been an Associated Professor with Syktyvkar University. He is the author of two books in Russian: *Polynomial Splines* (with V. N. Malozemov) (St. Petersburg, 1986) and *Multivariate Natural Splines* (with M. I. Ignatov) (St. Petersburg, 1991).

Valery A. Zheludev received the M.S. degree in 1963 from St. Petersburg University, St. Petersburg, Russia, and the Ph.D. degree from Steklov Mathematical Institute of the Academy of Sciences of the USSR, Steklov, Russia, in 1968, both in mathematical physics. In 1991 He received the Dr.Sci. degree in computational mathematics from the Siberia Branch of Academy Sciences of the USSR.

From 1963 to 1965, he was a lecturer at Pedagogical University, St. Petersburg, from 1965 to 1968, he was a Ph.D. student at St. Petersburg University, from 1968 to 1970, he was an Assistant Professor at Kaliningrad University, from 1970 to 1975, he was a Senior Researcher with the Research Institute for Electric Measuring Devices, St. Petersburg, from 1975 to 1995, he was an Associate and then a Full Professor at St. Petersburg Military University for Construction Engineering, and from 1995 to the present, he has been a Researcher then a Senior Researcher with the School of Computer Science, Tel-Aviv University, Tel-Aviv, Israel. He has also been with Paradigm Geophysical LTD, Tel-Aviv. His fields of research include wavelet analysis, approximation theory, signal and image processing, geophysics, and pattern recognition.

Dr. Zheludev received the prize for the best Ph.D. thesis at St. Petersburg University.